https://doi.org/10.6113/TKPE.2019.24.6.419

PMSG 풍력발전기용 3L ANPC와 TNPC 컨버터에서의 10kV IGCT 성능 비교 평가

암리나 라마 링도[1], 서용석[1], 박병건[2], 김지원[2]

Comparative Performance Evaluation of 10kV IGCTs in 3L ANPC and TNPC Converters in PMSG MV Wind Turbines

Amreena Lama Lyngdoh[1], Yongsug Suh[1], Byoung-Gun Park[2], and Jiwon Kim[2]

Abstract

Several multilevel converter topologies have been proposed and compared. The three-level (3L) neutral-point-clamped (NPC) topology is promising and widely accepted. However, this topology suffers from uneven loss distribution among switches due to its fixed switching strategy. The 3L active NPC (ANPC) topology, which exhibits improved loss distribution profile, was proposed to address this disadvantage. The 3L T-NPC topology, a hybrid configuration of 2L and 3L NPC topologies, was introduced to address not only the loss distribution problem but also the reduction in the number of switches. In the present research, the application of these three topologies in PMSG-based medium-voltage wind turbines was investigated. The power devices considered were 10 kV IGCTs. Performance was evaluated in terms of a power loss of 10 kV IGCT for each NPC topology, which is a crucial indicator of thermal behavior, reliability, cost, and lifetime of any converter. The comparison was performed using ABB make 10 kV IGCT 5SHY17L9000 and the simulation tool PLECS.

Key words: 3L ANPC, 10kV IGCT, Loss distribution, TNPC

1. Introduction

The multilevel converter topology provide unique solutions to work in high power applications. Amongst all the numerous multilevel converter structures, the 3L NPC is one of the widely accepted topology because of its superior performance in terms of output voltage quality, reduced switch power losses, harmonic distortion and common mode voltage/current[1].The 3L NPC in back to back configuration for PMSG wind turbine system is presented in Fig. 1. However, this topology suffers from uneven switching stress and loss distribution for each power device. Due to this over and underutilization of switches, switching frequency, maximum achievable power and even the reliability of the converter is restricted. The Active NPC (ANPC) topology which is a derivation from NPC was proposed to resolve this issue[2]. As compared to the NPC topology, the ANPC topology features two additional switches across the clamping diodes. One of the noticeable disadvantage of ANPC or NPC topology is the number of semiconductor components.

The 3L T-type NPC (TNPC) displays the structural behaviour of 2L converter and operational characteristics of 3L NPC converter. This topology use fewer power electronic switches while still giving the same 3L output voltage waveform as 3L NPC or ANPC converter[3],[4].

Paper number: TKPE-2019-24-6-5
Print ISSN: 1229-2214 Online ISSN: 2288-6281
† Corresponding author: ysuh@jbnu.ac.kr, Dept. of Electrical Eng., Chonbuk Nat'l University
Tel: +82-10-6628-5431 Fax: +82-632-270-2394
[1] Dept. of Electrical Eng., Chonbuk Nat'l University
[2] Korea Electrotechnology Research Institute
Manuscript received Apr. 25, 2019; revised May 20, 2019; accepted Jul. 9, 2019

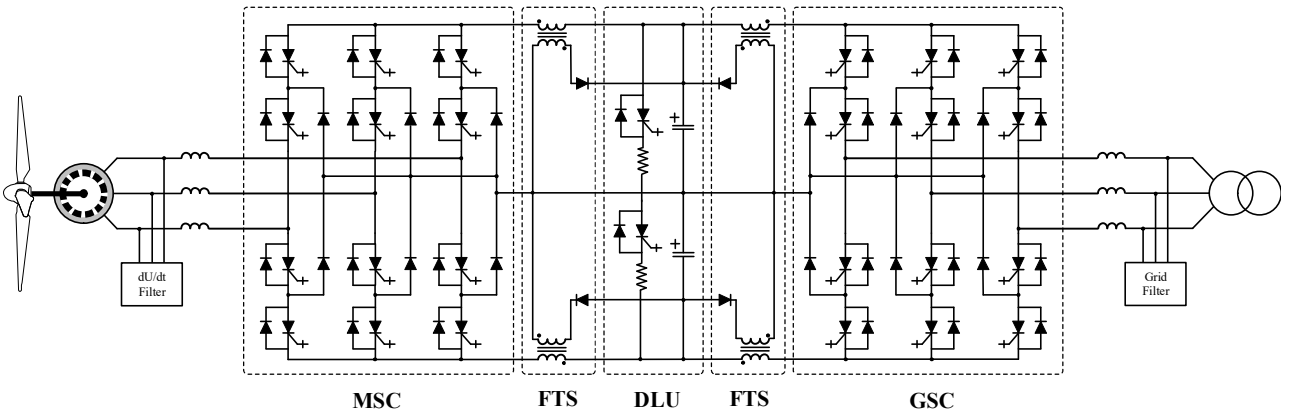

Fig. 1. A typical multilevel converter back to back configuration for 5MW PMSG MV wind turbine.

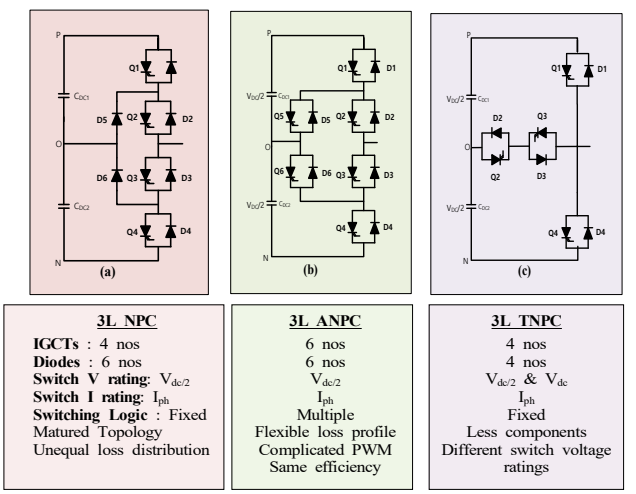

Fig. 2. Basic topology comparison.

With the wind turbine pushing its output capability to higher power limits, 10kV IGCT[5] will play an important role. Power converter failure is also a major reason for wind power plant downtime. Device failures are often due to device aging caused by thermal stress. It is therefore important to evaluate loss and the loss profile in a converter to ensure to the extent possible the even distribution of thermal stress amongst the individual switches[6]. Very limited research is available on loss distribution of 3L ANPC as well as TNPC converters, further no investigations are available for 10kV IGCT used in 3L ANPC and TNPC topology. This paper investigates the performance of 10kV IGCT in 3L ANPC - with four different modulation techniques and TNPC. Comparisons are made with the conventional NPC topology.

This paper is structured in the following manner. Section 2 describes the difference in the operation of 3L NPC, 3L ANPC and 3L TNPC. Brief description on the switching strategies of these topology are also presented under this section. The 10kV IGCT[3] under investigation and the loss model are presented in Section 3 followed by simulation parameters and performance comparisons of the 10kV IGCTs for 3L NPC, 3L ANPC and 3L TNPC in Section 4. Conclusions are given in Section 5.

2. Three Level NPC, ANPC and TNPC

2.1 Basic comparison of the 3L converters

Single leg of 3L NPC, ANPC, TNPC and a basic initial comparison of these topology are presented in Fig. 2. As can be seen from the figure the number of power semiconductor switches used for each topology is different. It is also interesting to note that while power devices in NPC and ANPC has switch voltage rating of Vdc/2, the TNPC topology consist of hybrid switches - wherein two outer switches are rated to withstand full dc link voltage Vdc and the two neutral point clamping switches are rated for half dc link voltage Vdc/2. The NPC and TNPC operations are based on identical but fixed switching logics however there are multiple switching strategies for ANPC[7],[8]. Consequently, ANPC has improved loss distribution profiles as compared to NPC. While both 3L NPC and 3L TNPC has fixed loss distribution, TNPC has better efficiency then 3L NPC due to the use of lesser components.

2.2 Switching strategies

Single leg of 3L NPC topology is represented by Fig. 3. In this conventional topology, to achieve the positive state(P), the top switches Q_1 and Q_2 are switched on as indicated in Fig. 3(a) and for the negative state(N), the bottom two switches Q_3 and Q_4

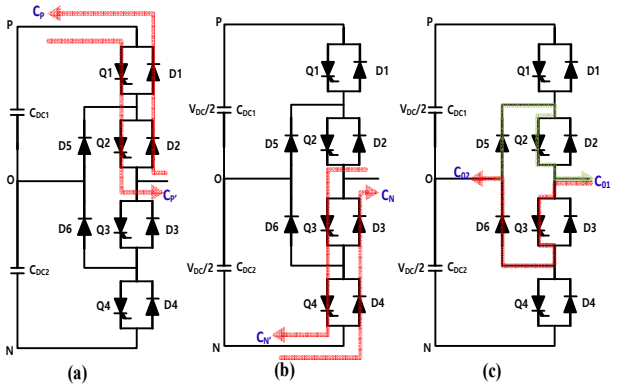

Fig. 3. Operation of 3L NPC.

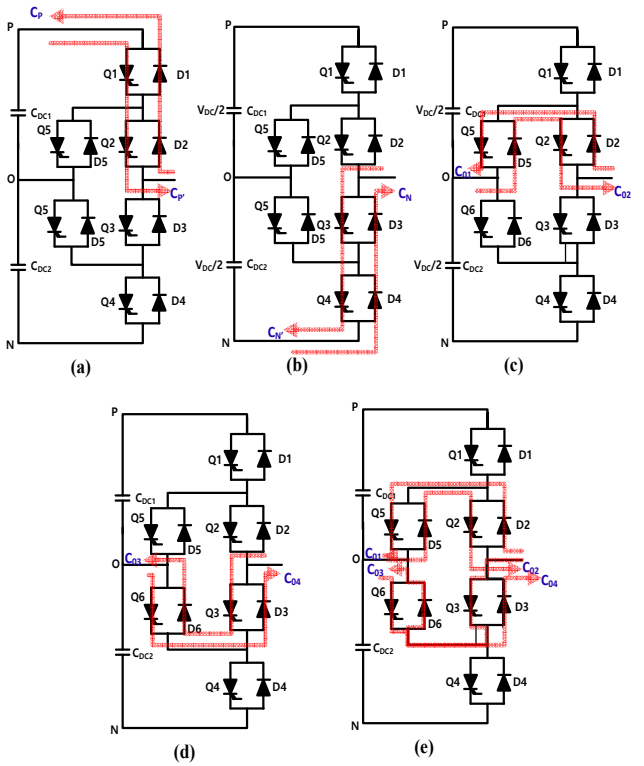

Fig. 4. Operation of 3L ANPC.

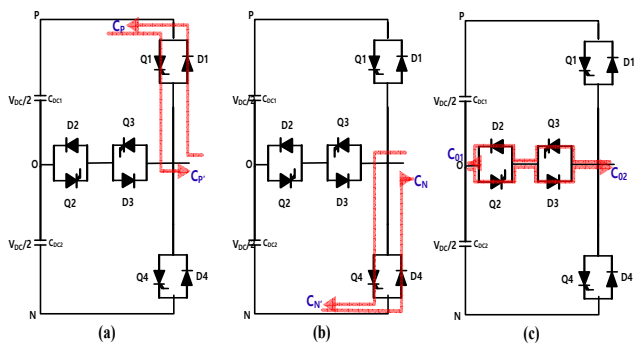

Fig. 5. Operation of 3L TNPC.

are turned on as shown in Fig. 3(b). For the neutral state(0), the current direction determines the path and therefore both switches Q_2 and Q_3 are turned on as represented in Fig. 3(c). The current paths C_P, $C_{P'}$, C_N, $C_{N'}$ C_{01} and C_{02} defines the inverter or rectifier mode of operation. The NPC topology provides six different current paths and has only one switching strategy for P, 0 and N states.

Fig. 4 shows the single leg of 3L ANPC topology composed of six bidirectional switches. Like 3L NPC topology, for P state switches Q_1, Q_2 and for N state switches Q_3, Q_4 are turned on as indicated by Fig. 4(a) and 4(b). However in some of the switching strategies of ANPC switches Q_6, Q_5 are lso kept turned on during the P and N state respectively for equal voltage distribution between the off state switches. As shown in Fig. 4(c) to 4(e), the zero state in case of ANPC topology can be realized in multiple ways - the upper path(Q_2, Q_5 turned on) - short switching loop (SSL) of the clamping point, the lower path(Q_3, Q_6 turned on) - long switching loop (LSL) of the clamping point, both the upper and lower path(Q_2, Q_3, Q_5, Q_6 turned on) - Only One Zero State (OOZS) and finally the doubled frequency (DF)[4] where both SSL and LSL are used alternatively in one switching period, achieve the zero state. Based on the output voltage and current direction, the ANPC topology provides eight different current paths as shown in Fig. 4(a) to (d). The multiple option to implement the neutral current paths (C_{01}, C_{02}, C_{03}, C_{04}) enables more variety in the modulation strategies.

Fig. 5 presents the single leg of 3L TNPC topology composed of four bidirectional switches. Like 3L NPC topology, for P state switches Q_1, Q_2 and for N state switches Q_3, Q_4 are turned on respectively as indicated by Fig. 5(a) and 5(b).For the neutral state(0), both switches Q_2 and Q_3 are turned on as indicated in Fig. 5(c). Depending on current direction, one of the current paths C_{01} or C_{02} is used.

3. 10kV IGCT and Loss Model

10 kV IGCT device has been launched recently and its switching capability confirmed[9],[10]. This device can be applied in the voltage class of 6-7.2kV MV 3L VSCs without the conventional series connection technique. When compared with the power component count of series connected 4.5kV or 5.5kV IGCT device, the use of 10kV IGCT device contributes to a total reduction of device count by 41-71%. Table I presents the characteristic specifications of the semiconductor devices - 10kV IGCT and 10kV Diode.

TABLE I
DEVICE SPECIFICATIONS

Device	Parameter	Value
IGCT	Blocking Voltage	9kV
	$I_{TGQM}/I_{F(AV)}$	1700A
	V_{on}	2.2V
	R_{on}	1.2mΩ
	E_{on}(5kV/1.7kA)	1.5J
	E_{off}(5kV/1.7kA)	19.5J
	T_{vj_max}	125°C
	$R_{th(j-c)}+R_{th(c-h)}$	(9.5+3) K/kW
Diode	Blocking Voltage	9kV
	$I_{TGQM}/I_{F(AV)}$	1700A
	V_{on}	2.2V
	R_{on}	1.6mΩ
	E_{on}	-
	E_{off}(5kV/1.7kA)	22J
	T_{vj_max}	125°C
	$R_{th(j-c)}+R_{th(c-h)}+R_{th(h-a))}$	(6+3+6) K/kW

The given data is employed in the loss calculation of the three multi-level converters described in the previous section.

Simplified loss estimation model[11],[12] is shown in Fig. 6[9]. The approximate analytical expressions for power in terms of voltage and current used to calculate the losses of the IGCT are represented by equation (1) to (3). Semiconductor device loss comprises of switching loss and conduction loss. The switching losses of IGCT as shown in Fig. 6(a) & (b) are calculated using the total commutation time during which the IGCT turns on/off, the voltage v(t) and current i(t) of the IGCT. The average switching loss maybe computed by adding all the commutations of the IGCT over the respective interval of time.

The conduction loss of each switch is a function of instantaneous voltage $V_{sw}(t)$ and the instantaneous current i(t). As indicated in Fig. 6(c) $V_{sw}(t)$ can be linearly approximated as function of threshold voltage V_{on} and series resistance R_{on}. If E_{on} and E_{off} are the energy dissipated during IGCT turn on and turn off then switching loss during turn on and turn off can be represented in expressions given in (1) & (2) and

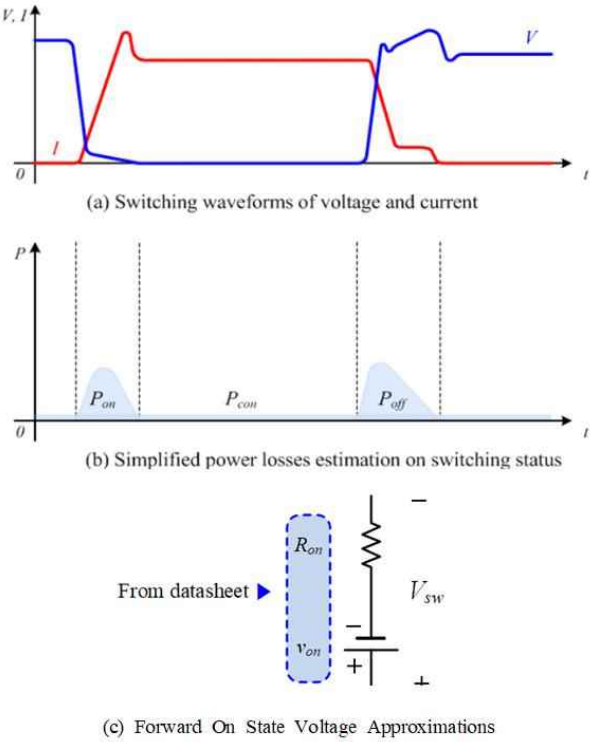

Fig. 6. Loss model of semiconductor device.

provides the linear approximation of the actual switching loss based on specific values of E_{on}(spec) and E_{off}(spec) given by the manufacturer. The loss calculated is found to be fairly accurate, particularly within the vicinity of the manufacturer's test point (V_{test} and I_{test})[9]. The total conduction loss in IGCTs can be represented by the equation (3) given below.

$$P_{loss\_on} = E_{on} \times f_{sw} = \frac{V_{on(measure)}}{V_{test}} \times \frac{I_{on(measure)}}{I_{test}} \times E_{on(spec)} \times f_{sw} \quad (1)$$

$$P_{loss\_off} = E_{off} \times f_{sw} = \frac{V_{off(measure)}}{V_{test}} \times \frac{I_{off(measure)}}{I_{test}} \times E_{off(spec)} \times f_{sw} \quad (2)$$

$$\begin{aligned} P_{cond} &= \frac{1}{T}\int v_{sw}(t)i(t)dt \\ &= \frac{1}{T}\int \{v_{on} + R_{on}\cdot i(t)\}i(t)dt \\ &= v_{on}I_{C\_AVG.} + R_{on}\left(I_{C\_RMS}\right)^2 \end{aligned} \quad (3)$$

4. Simulation Parameters and Results

4.1 Simulation conditions

The simulations operation parameters based on 5MW MV grid side and machine VSCs are given in the Table II. Grid side switching frequency is dominated by the optimal selection between the

TABLE II
SIMULATION PARAMETERS

Parameter	Symbol	Value
Output Power	$P_{rated-out}$	5 MW
Grid Frequency	f_{grid}	60 Hz
Grid side inductance	L_{grid}	1.56mH
Grid side input voltage	V_{LL}	4.16kV
Grid side input current	I_{AC_input}	708 A
Switching Frequency	f_{GSC_PWM}	1020 Hz
DC-link voltage	$V_{DC-link}$	7 kV
DC-link Capacitance	$C_{DC-link}$	2.6 mF
AC filter inductance	L_f	1.5 mH
AC filter capacitance	C_f	0.35 mF
di/dt limiting inductance	L_i	4μH
PMSG Output	$PMSG_{rated\_out}$	5 MW
Machine side Frequency	f_{pmsg}	29.1 Hz
Machine side input voltage	$V_{LL(PMSG)}$	6.9kV
Rated stator current	I_{stator}	920 A

switching loss and harmonic content of ac input current. Loss calculation is based on the parameters given in Table I and Table II. The losses are calculated under the condition of maximum ac input current, line under-voltage of 90% and power factor of 0.9 leading by sampling each switching instant of the 10kV IGCT as shown in Fig. 7.

4.2 Results and analysis

Loss profile of 10 kV IGCT used in grid side converter (GSC) and machine side converter (MSC) with 3L NPC, ANPC and TNPC topology in 5 MW PMSG MV wind turbines under 0.9 leading power factor are represented by Fig. 8 and 9 respectively. These figures summarize the switching and conduction loss data for the complete 3-phase legs in a total system of 5MW GSC and MSC with fixed switching logic for NPC and TNPC topology however for ANPC topology, loss is presented with four different switching strategies as described in previous section. The turn on losses of anti-parallel as well as clamping diodes are found to be negligible and hence not considered in this paper. Also, the small losses incurred by devices commuting during the time interval between switch turn on and off period as

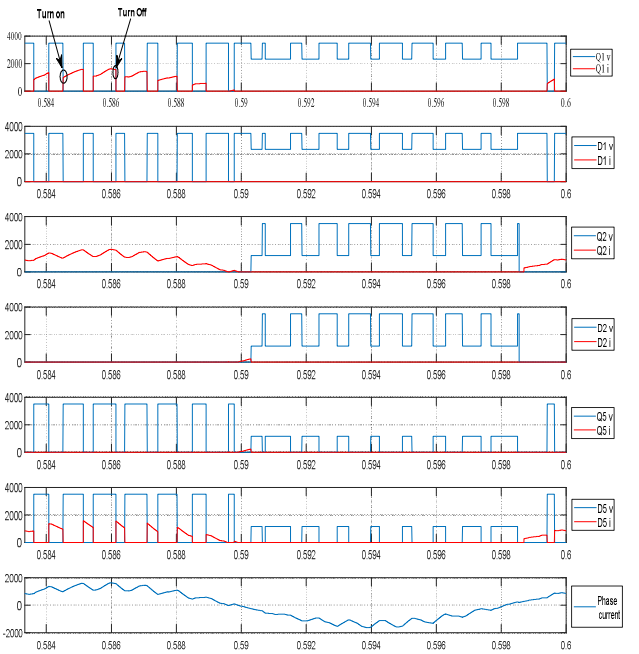

Fig. 7. Switching instant of IGCT - Upper leg(3L ANPC).

well as during zero crossing is not presented in this paper. Only the major losses in devices which actively participate in switching and commutation are presented and discussed. Clearly the loss distribution characteristics of GSC is different from MSC for all the three converters.

As can be seen from the figure, in 3L NPC GSC the outer switches Q_1, Q_4, D_5 & D_6 generate the maximum loss while the inner switches Q_2 & Q_3 dissipate only conduction loss. In the GSC mode the active switches and its commutations sequence is either from Q_1/Q_2 to D_5/Q_2 or Q_3/Q_4 to D_6/Q_3 depending on voltage state and current direction. As can be seen both commutations use the shortest commutation paths. It may also be observed that Q_1/Q_4 switch at carrier frequency while Q_2/Q_3 is turned on for half line frequency period each, consequently avoiding switching loss and dissipating only conduction loss as is shown in the figure. The GSC -SSL PWM technique generate loss profile identical to 3L NPC GSC since these switching logic use only shortest commutation paths. The GSC-LSL technique redistributes the loss to the inner switches (Q_2, Q_3, D_2 & D_3). With LSL PWM conduction losses are shared amongst the inner and outer switches because of non-sharing of same device for current path, which is not true for SSL-PWM where Q_2 is shared to attain positive state as well as neutral state. In the GSC mode the active switches and its

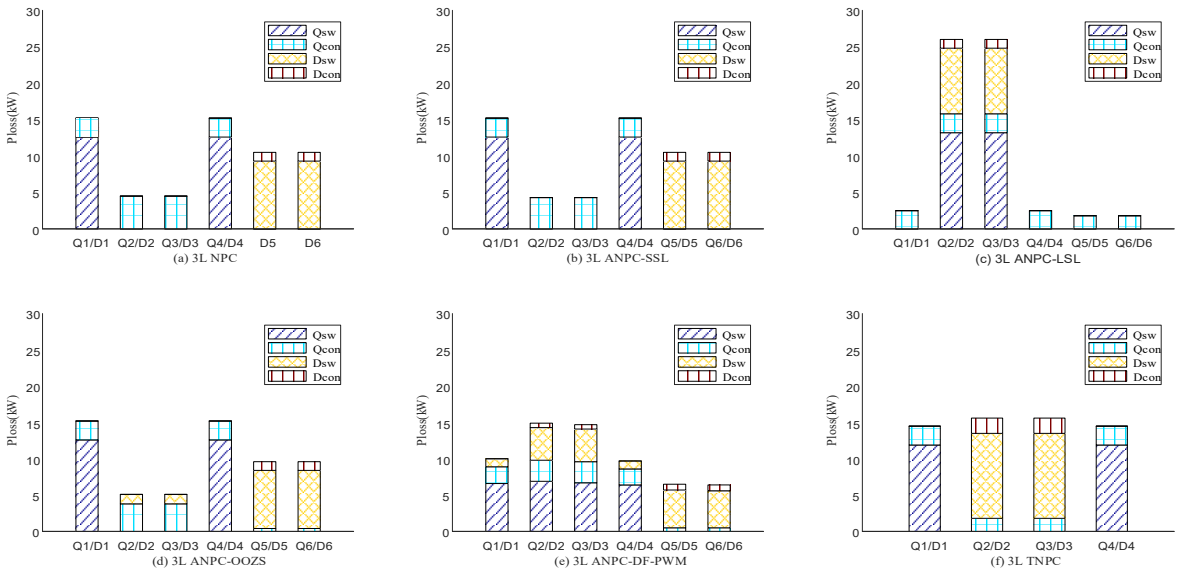

Fig. 8. Loss distribution of grid side converter using 3L NPC, ANPC and TNPC in 5MW PMSG MV wind turbine plant.

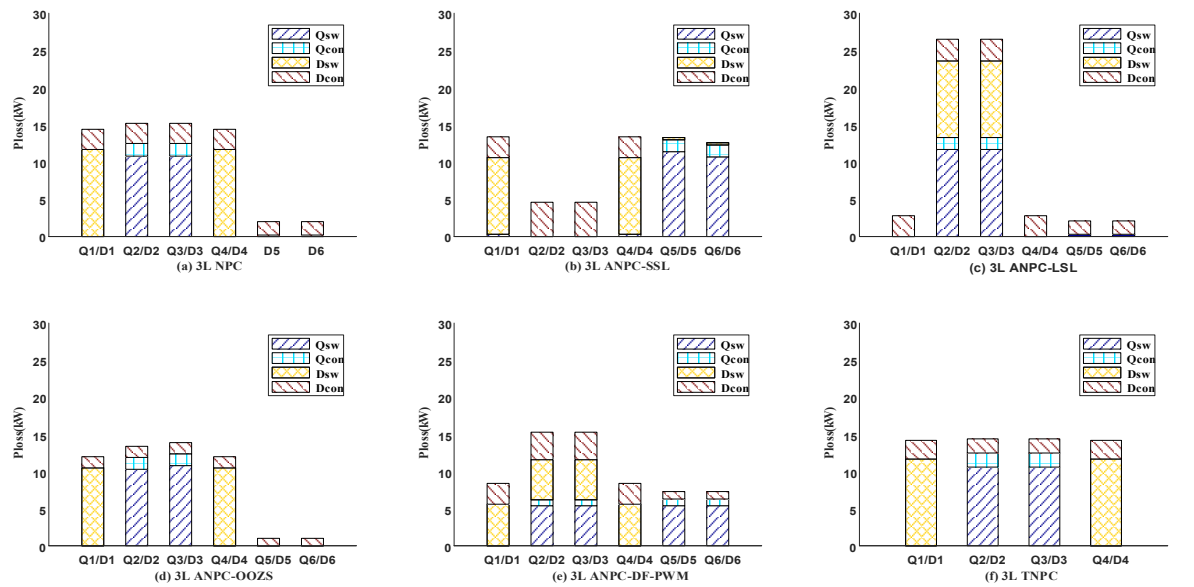

Fig. 9. Loss distribution of machine side converter using 3L NPC, ANPC and TNPC in 5MW PMSG MV wind turbine plant.

commutations sequence for LSL based switching strategy is either from Q_1/Q_2 to D_3/Q_6 or Q_3/Q_4 to D_2/Q_5 and therefore the switching losses are experienced only by the inner switches as can be seen from Fig. 8. Additionally, it maybe observed that only the long commutation paths are used hence the name long switching loop(LSL) PWM. With OOZS PWM, all the inner switches are turned on to achieve the zero state. Some of the losses from the clamping devices are dispersed to the inner switches. However the switching loss remains the same as 3L NPC. As reflected in Fig. 8, the switching losses are well distributed amongst all the four inner switches (Q_1, Q_2, Q_3, Q_4) in case of DF PWM. This switching strategy use both short switching loop and long switching loop within one carrier period. This enables the natural doubling of the apparent switching frequency of the output pole voltage. Therefore to generate output voltage with frequency same as other PWMs, the carrier switching frequency in case of DF-PWM is considered half of other PWMs. This is an important advantage of this PWM.

Loss behaviour of the 3L TNPC is fixed unlike ANPC. The switching characteristics of Q_1 and Q_4 are identical to the NPC however the uniqueness of neutral point path is the use of two switches which

TABLE III
COMPARISON TABLE

GRID SIDE CONVERTER					
Topology	Strategy	Total Loss (KW)	Max Loss of a Device(KW)	Efficiency(%)	Most Stressed Devices
NPC		60	5	98.79	Outer
ANPC	SSL	60	5	98.80	Outer
ANPC	LSL	61	5.2	98.78	Inner
ANPC	OOZS	60	5	98.80	Outer
ANPC	DF-PWM	62	3.4	98.75	Inner
TNPC		60	4.8	98.80	Outer

MACHINE SIDE CONVERTER					
Topology	Strategy	Total Loss (KW)	Max Loss of a Device(KW)	Efficiency(%)	Most Stressed Devices
NPC		63	4.8	98.74	Outer
ANPC	SSL	62	4.3	98.76	Outer
ANPC	LSL	63	4.4	98.74	Inner
ANPC	OOZS	63	4.4	98.74	Outer
ANPC	DF-PWM	62	3.3	98.76	Inner
TNPC		58	4.8	98.84	Outer

share the load. By keeping Q_2 on during P state or Q_3 on during the N state each switch experience switching loss only in half of each voltage period.

The loss distribution profile for MSC for all the three topology is presented in Fig. 9. As can be clearly seen for generator side converter the diodes dissipate more power loss than the IGCTs.

It is interesting to note that unlike GSC, in the 3L NPC MSC only long commutation paths are used. In the MSC, the active switches and its commutations sequence is either from D_1/D_2 to D_6/Q_3 or D_3/D_4 to D_5/Q_2 depending on voltage state and current direction. Hence the losses can be observed in the outer Diodes and inner IGCTs as reflected in the figure above for 3L NPC MSC.

In SSL- PWM, the clamping switches and the inner diodes take on the switching loss unlike the LSL-PWM where the losses of the clamping switches are dispersed to the inner switches(Q2 & Q3). However as in GSC-LSL, the conduction losses in MSC-LSL PWM are also well spread amongst the switches. The loss profile of the devices using OOZS PWM shows a combination of the SSL & LSL PWM loss profiles.

Like GSC-DF PWM, the losses in MSC-DF PWM are extended to all the switches and diodes. As stated earlier, due to two active states within one switching period in the DF PWM technique, the output voltage switching frequency has an apparent switching frequency equal to twice the switching frequency.

Table III above represents the performance of the three topology operating as grid side and machine side converters. This table includes some of the important performance parameters of 3L NPC, ANPC and TNPC topology. As can be seen the from the table the maximum loss and thermal stress of the10kV IGCT switches under each topology and switching method is different. It maybe noted that the efficiency of the converter is approximately same for grid side operations for all topology however more machine side converter, the losses are higher due to the high loss of 10kV Diode which has a higher E_{off} then the 10kV IGCT consequently leading to poorer efficiency as compared to grid side operations.

5. Conclusions

In this paper, loss analysis of 10kV/1700A IGCT for 5MW MV wind turbine employing 3L ANPC BTB VSC is investigated. The output power limit, cooling system size, reliability and lifetime of power converter is dependent on the thermal behavior of the 3L ANPC VSC. In this paper the loss behaviour of the 10kV IGCTs are studied for three different topology and for Generator side and Grid side converters. Four different PWM strategies are used for 3L ANPC and different loss profiles are produced. Clearly the switching techniques influence the power

loss distribution inside the 3L ANPC topology unlike 3L NPC and TNPC. Through this comparative research of the three topology it maybe concluded that 3L TNPC exhibits very simple structural operational behaviour however the switch loss profile is not much improved. In 3L ANPC amongst the four modulation methods, it maybe concluded that the DF-PWM technique portray the best loss sharing profile. However, the classical PWM techniques are easier to implement when compared to DF-PWM implementation.

This research was supported by the Korea Electrotechnology Research Institute (KERI) Primary research program of MSIT/NST (No. 19-12-N0101-36)

References

[1] I. T. Nabae and H. Akagi, "A new neutral-point-clamped PWM inverter," *IEEE Trans. Industrial Applications*, Vol. IA-17, No. 5, pp. 518-523, May 1981.

[2] P. S. Barbosa, P. Steinke, J. Meysenc, M. L. Winkelnkemper, and N. Celanovic, "Active neutral-point-clamped multilevel converters," in *2005 IEEE Power Electronics Specialists Conference*, pp. 2296-2301, Jun. 2005.

[3] M. Schweizer and J. W. Kolar, "High efficiency drive system with 3-level T-type inverter," in *2011 IEEE International Power Electronics and Motion Control Conference (ECCE Europe 2011)*, pp. 1-10, Aug. 2011.

[4] M. Schweizer and J. W. Kolar, "Design and implementation of a highly efficient three level t-type converter for low-voltage applications," *IEEE Trans. on Power Electronics*, Vol. 28, No. 2, pp. 899-907, Feb. 2013.

[5] I. Nistor, T. Wikstrom, and M. Scheinert, "IGCTs: High-power technology for power electronics applications," in *2009 International Semiconductors Conference*, Vol. 1, pp. 65-73, Oct. 2009.

[6] Y. Suh, J. K. Steinke, and P. K. Steimer, "Efficiency comparison of voltage-source and current-source drive systems for medium-voltage applications," *IEEE Trans. Industrial Electronics*, Vol. 54, No. 5, pp. 2521-2531, Oct. 2007.

[7] Y. Jiao and F. C. Lee, "New modulation scheme for three-level active neutral-point-clamped converter with loss and stress reduction," *IEEE Trans. Industrial Electronics*, Vol. 62, No. 9, pp. 5468-5479, Sep. 2015.

[8] D. Floricau, E. Floricau, and M. Dumitrescu, "Natural doubling of the apparent switching frequency using three-level ANPC converter," in *2008 International School on Non-sinusoidal Currents and Compensation*, pp. 1-6, Jun. 2008.

[9] S. Bernet, E. Carroll, P. Streit, O. Apeldoorn, P. Steimer, and S. Tschirley, "Design, test and characteristics of 10kV IGCTs," in *2003 IAS Annual Meeting on Conference Record of the Industrial Applications Conference*, Vol. 2, pp. 1012-1019, Oct. 2003.

[10] C. Thomas and B. Bjorn, "High power IGCT switches-state-of-the-art and future," in *2011 Power Electronics Europe*, PCIM:12-408/506, No. 3, pp. 30-34, 2011.

[11] K. Lee, K. Jung, Y. Suh, C. Kim, H. Yoo, and S. Park "Comparison of high-power semiconductor devices losses in 5MW PMSG MV wind turbines," in *2014 Applied Power Electronics Conference and Exposition (APEC)*, pp. 1048-2334, Mar. 2014.

[12] S. Shirmohammadi, K. Lee, and Y. Suh, "Low dissipative snubber using flyback type transformer for 10kV IGCT in 7 MW wind turbine systems," *IEEE Trans. on Power Electronics*, Vol. 33, No. 7, pp. 5898-5908, Jul. 2018.

Amreena Lama Lyngdoh

She was born in Assam, India. She received the B.S. degree in Electrical Engineering from National Institute of Technology, Silchar, India in 2005. She worked in Bharat Heavy Electricals Limited from 2005 to 2014. From 2016 to 2019 she was a Master's Degree Research Student in the Environment Friendly Energy Conversion Laboratory of Chonbuk National University, Jeonju, South Korea.

Yongsug Suh

He was born in Seoul, Korea. He received the B.E.E and M.S.E.E degrees from Yonsei University, Seoul, Korea, in 1991 and 1993 respectively, and the Ph.D. in Electrical Engineering from the University of Wisconsin, Madison, in 2004. From 1993 to 1998, he was an Application Engineer in the Power Semiconductor Division of Samsung Electronics Co. Korea. From 2004 to 2008, he was a Senior Engineer in the Power Electronics & Medium Voltage Drives Division of ABB, Turgi, Switzerland. Since 2008, he has been with the Department of Elctrical Engineering, Chonbuk National University, Jeonju Korea, where he is currently an Assistant Professor. His research interests include power conversion systems of high power for renewable energy sources and medium voltage electric drive systems.

Byung-Gun Park

He received his B.S. in Electrical Engineering from Myongji University, Yongin, Korea, in 2005, and his M.S. and Ph.D. in Electrical Engineering from Hanyang University, Seoul, Korea, in 2007 and 2011, respectively. Since 2011, he has been with the Korea Electrotechnology Research Institute (KERI), Changwon, Korea, where he is currently a Senior Researcher in the Electric Motor Research Center.

Jiwon Kim

He received the B.S. degree from the University of Seoul, Seoul, South Korea, in 1994, and the M.S. degree from Kwang-Woon University, Seoul, South Korea, in 1996, both in control and instrumentation engineering, and the Ph.D. degree in electrical engineering from Pusan National University, Busan, South Korea, in 2014. Since 1996, he has been with the Electric Motor Research Center, Korea Electrotechnology Research Institute, Changwon, South Korea.